Essential Readings in Light Metals: Electrode Technology for Aluminum Production.
Edited by Alan Tomsett and John Johnson.

From ***Light Metals 1982***, J.E. Andersen, Editor

PENETRATION OF SODIUM AND BATH CONSTITUENTS INTO CATHODE CARBON MATERIALS USED IN INDUSTRIAL CELLS

Conrad Krohn, Morten Sørlie and Harald A. Øye

Institutt for uorganisk kjemi
Universitetet i Trondheim
Norges tekniske høgskole
N-7034 Trondheim-NTH, Norway

To elucidate further upon possible mechanisms of reaction leading to a shortened life-time of the carbon lining in aluminium reduction cells, two commercially available cold type seam mixes have been tested with respect to penetration of sodium and bath constituents into the material. Testing conditions were kept close to what may be expected in the cathodic part of industrial cells in operation. The Type I seam mix consisted of anthracite with a substantial amount of graphitic material and a binder which during baking gave a soft, porous coke. The Type II was an amorphous anthracite mix with an aromatic binder giving a high crushing strength coke during baking.

The materials were subjected to sodium vapour and sodium generated during electrolysis in a melt with a commercial bath composition and a varying cryolite ratio. The resulting exposed material was investigated employing X-ray methods and microprobe analysis. Pore volume and pore size distribution was also recorded.

In spite of its inferior crushing strength, the Type I material was superior to Type II with respect to cracking and desintegration when exposed to sodium under conditions which may exist in aluminium reduction cells. When a cathodic potential is applied to the carbon, a sodium wave will first pass through the material followed by the migrating electrolyte which only has access to the porous part of material. The reaction with sodium, which in itself may result in a desintegration of especially non-graphite material, also probably changes the wetting characteristics of the carbon material, thus enabling the bath to penetrate.

Introduction

The most frequent cause of forced shut-down of aluminium reduction cells is problems arising in connection with the cathodic part of the cell. This can usually be attributed to the carbon lining, such as a long-term degradation or deformation of the lining itself. This in turn may cause a sudden increase in iron content of the metal due to the exposure of a current collector bar, or a catastrophical tap-out of metal and electrolyte through the bottom or the side lining. The causes leading to the deterioration of carbon linings have been discussed (1) in terms of compounds formed in the cathode bottoms and possible penetration and failure mechanism during electrolysis.

In modern cells the carbon bottom consists of preformed and prebaked blocks made from calcined anthracite with a pitch binder. Due to good packing and high and uniform baking temperature (1100-1400°C) such cathode slabs are superior compared to the old monolithic cathodes in terms of resistance towards deterioration caused by penetration of sodium and electrolyte. The seams separating the cathode blocks are, however, weak points where penetration and erosion may occur. These seams are tamped with a seam mix which ideally should not be distinguishable from the surrounding blocks after baking. This is, however, not practically achievable and the seams are often characterized by lower density due to a relatively higher content of volatile matter before baking and from a lower and more uneven packing pressure (2). Volume change during baking is also very important. The adhesion between the seam mix and the prebaked carbon slabs may be weaker than within the seam itself. As the apparent "green" density is lower than that of the block, shrinkage can be substantial, leading to gaps between seam and block. In later years cold seam mixes seem to have replaced hot melt mixes. The former can be applied at room temperature, produce less noxious emissions, reduce the installation cost and have a higher "green" apparent density when installed (3). Laminations are avoided because cooling does not prevent successive batches of seam mix from blending together during tamping.

The inhomogeneity of the seam, compared to the denser and more homogeneous cathode block, is clearly illustrated in Figure 1 (4). This shows a core

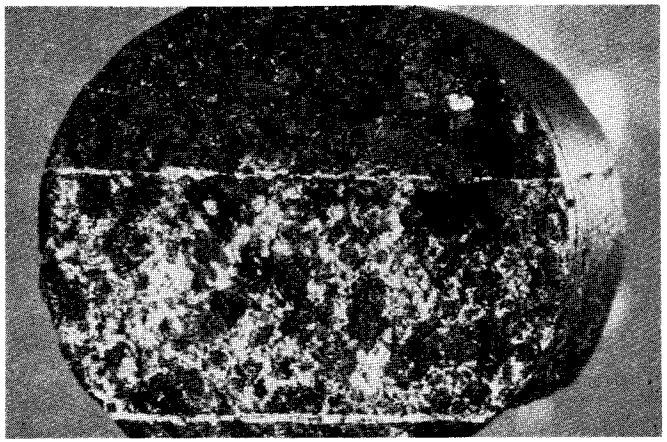

Fig. 1. Core sample from a failed prebaked cathode type cell shows prebaked block (upper and lower part) and seam (middle part). The "white" phase seen throughout the seam is mainly Na_3AlF_6, NaF and yellow Al_4C_3 (4).

taken from a 3 cm wide seam in an industrial cell which has been taken out of production. The middle horizontal part of the core sample shows the seam. The "white" material which appears to fill every void and pore in the seam consists mainly of yellow aluminium carbide, cryolite and sodium fluoride. Al_4C_3 is readily formed when cathode carbon materials get into contact with cryolite and molten aluminium (5) or by the reaction between sodium, carbon and cryolite (6). The contrast between the seam and the prebaked block in Figure 1 is conspicuous and the lack of proper adhesion between block and seam mix can be seen.

The resistance of the carbon material towards sodium attack plays a significant role. The swelling of carbon during absorption of sodium (7) which in severe cases may lead to complete disruption and exfoliation of carbon bodies (8) has been demonstrated. Some disagreement exists in the literature concerning the mechanism of sodium penetration into cathode carbon materials. It may either take place as a vapour transport (9) through microcracks and the porous binder material or sodium may migrate by diffusion through the carbon lattice (6) and not predominantly through the pores.

This paper gives some results obtained during testing of two commercially available cold type seam mixes used in aluminium reduction cells. The testing conditions have been kept close to what may be expected in the cathodic part of operational aluminium cells.

Characteristics of the Carbon Materials

Aluminium smelters often formulate their own seam mix, but a number of types are also commercially available from companies specializing in carbonaceous materials. The different mixes may contain a variety of types of carbon and pitch, and exhibit a variable particle size distribution and pitch content. The carbonaceous material in cathode seam mixes is usually made up from anthracite, graphite or mixtures of these. Gas calcined anthracite has been fired to a relatively low temperature (1200-1400°C) where no substantial graphitization takes place. Electrically calcined anthracite may locally be subjected to temperatures of 2200-2400°C and a high degree of graphitization may be obtained.

In order to study the influence of graphitic materials in the seam mixes we have chosen to work with two makes of cold type seam mixes from different manufacturers, both commercially available and in the following denoted Type I and Type II, respectively. Some characteristic parameters of the two different seam mixes are given in Table 1. Type I consists of anthracite containing a substantial amount of graphitic material, while Type II is a very amorphous anthracitic mix. This is evident from the X-ray reflections from the (002) plane in the latter material (Fig. 2). Another difference between the mixes is the binder. The binder in Type I consists of a heavy oil fraction which upon baking gave a soft, porous coke resembling petrol coke. Type II binder contains a substantial amount of aromatic components and produced a very hard glass-like coke by pyrolysis. This is evident from the crushing strengths given in Table 1.

A rough particle size distribution for Type I and Type II mixes is given in Table 2. Both types contain about the same amount of very fine (<211μm) and very coarse particles (>4699μm), and only the particle size distribution of the intermediate fractions appears to differ somewhat.

The test specimens were cylinders made by compacting the mix at a pressure of 850 bar. This pressure is considerably higher than what is obtain-

Table 1. Characteristic properties of the two types of seam mixes.

Property	Type I	Type II
Binder content	12.0 %	10.3 %
Ash content (baked)	1.9 %	4.4 %
Weight loss during baking	9.1 %	6.1 %
Density (baked)	1.50 g cm^{-3}	1.41 g cm^{-3}
Porosity (baked)	18.6 %	14.4 %
Crushing strength (baked)	150 bar	600 bar

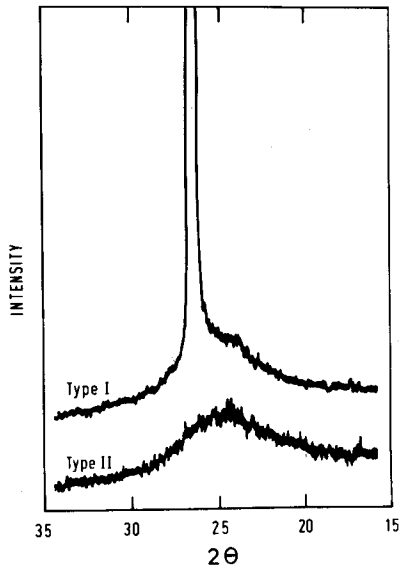

Fig. 2. X-ray diffraction curves of Type I (top) and Type II (bottom) unbaked seam mixes. The scans include the (002) region in graphite.

Table 2. Particle distribution in the two seam mixes.

Sieve aperture μm	Type I %	Type II %
+4699	3.1	4.0
-4699 to +2030	27.3	14.9
-2030 to +853	17.9	15.7
-853 to +211	18.5	32.4
-211	33.1	32.9
	99.9	99.9

able during packing of seam mixes in industrial cells but was chosen because in this pressure range the porosity of the specimens is independent of pressure. The baking took place in a nitrogen atmosphere. The temperature was raised from ambient to 1000°C at a rate of 80°C/h followed by a holding time of 12 h at the upper temperature.

Deterioration Due to Sodium Vapour

Alkali metal vapours are known to cause extensive swelling and cracking of carbon materials (10,11). Some carbons are known to form intercalation compounds with sodium as well as with the other alkali metals and stoichiometric compounds such as $C_{64}Na$ (12) and $C_{12}Na$ (13) have been reported. The intercalating atoms forces the carbon layers apart and swelling results. The intercalation may be followed by catastrophic crack propagation which in well ordered graphite cylinders have resulted in the material being split up in discrete discs (14).

The driving force for sodium intercalation into carbon is the charge transfer between the intercalating atoms and the π-bond system of the carbon. A low Fermi level as found in anthracite and other carbons of low order will favour an electron transfer to the carbon. Sodium atoms which are strong electron donors will therefore readily react with anthracite, while graphite which has a higher Fermi level thus preferring electron acceptors as intercalants, will be expected to be less reactive. Moreover, sodium is found to intercalate with a preference for those parts of the structure where the interlayer distances are significantly larger than in well crystallized graphite (13).

The effect of sodium vapour on Type I and Type II seam mixes is demonstrated in Figure 3. The two baked specimens (15 mm diameter x 30 mm high) were kept at 883°C (boiling point of Na) under 1 atm of sodium vapour. The carbon cylinders and sodium were contained in a stainless steel autoclave for 3.5 h under the above conditions. The temperature gradient was made such that no liquid sodium, only vapour, was in contact with the carbon.

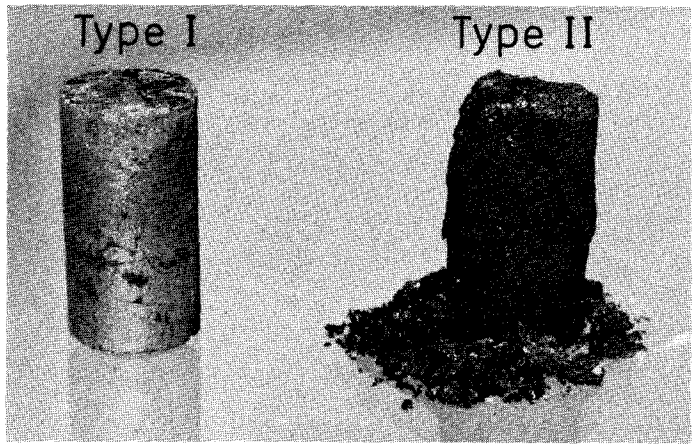

Fig. 3. Type I (left) and Type II (right) seam mix samples after being subjected to 1 atm sodium vapour at 883°C.

The Type I seam mix shows very little damage. It has retained its original shape and only a few hairline cracks are visible on the surface. The Type II cylinder, however, has completely disintegrated due to swelling and a catastrophic crack propagation throughout the carbon material can be observed.

Although the softer binder in the Type I mix may contribute to the better resistance towards sodium attack as it might stop crack propagation at the grain boundaries, the main reason for the improved performance of this seam mix is probably due to its content of graphitic material. The hard and amorphous anthracite grains in the Type II seam mix cracks easily when sodium penetrates the lattice. The very hard binder in these acts as a continuation of the anthracite grains as a catastrophic crack propagates throughout the material, as clearly demonstrated in Figure 3.

This could be verified in an experiment similar to the one described above where the binder phase had been extracted from and switched between the two mixes. To a portion of each type of seam mix was added dichloromethane. After thorough mixing soluble matter was removed by filtration. This procedure was repeated until all material soluble in dichloromethane was removed. When most of the solvent had evaporated the pitch fractions were again mixed with the dry coke so that Type I solids now contained the binder from Type II (Type I(II)) and *vice versa* (Type II(I)).

The results were almost identical to the first experiment with respect to cracking and swelling in the coke fractions. The Type I(II) mix showed only hairline cracks. The Type II(I) mix showed severe cracking with a swelling of ~10% along its axis. The exfoliation was, however, not as severe as for Type II mix, probably due to that the softer binder acted as a restraint to crack propagation across the grain boundaries.

Simulation of Cell Operating Conditions

Chemical generation of sodium

A sodium partial pressure of 1 atm can hardly be reached in an aluminium reduction cell, but Na is present at reduced activity due to the equilibrium:

$$Al(l) + 3NaF(\text{in cryolite}) = 3Na(\text{dissolved}) + AlF_3(\text{in cryolite}) \quad (1)$$

The sodium activity and thus the sodium content of aluminium in equilibrium with NaF-AlF_3 melts (15) will depend upon the cryolite ratio:

$$CR = \text{mol\% NaF} / \text{mol\% } AlF_3 \quad (2)$$

The acidity of the melt may be varied within wide limits by changing the CR, from extreme basicity in pure molten NaF to melts with high acidity containing excess AlF_3 relative to the neutral cryolite composition.

A modified Wilkening test (8) has been adapted to test the resistance of the two cold seam mixes against failure due to sodium penetration. Crucibles were made from pressed and fired cylinders of Type I and Type II cold seam mixes (Fig. 4). The wall was made sufficiently thin so that the effect of the CR on the carbon degradation could be demonstrated. The crucibles were 27 mm diameter x 55 mm with inner dimensions 16 mm diameter x 40 mm. A cylinder (15 mm diameter) consisting of finely dispersed Al-metal (6 g) and a cryolite mixture of the required CR (10 g) was compacted at a pressure of 550 bar and placed into the crucible. When molten, this may closely resemble

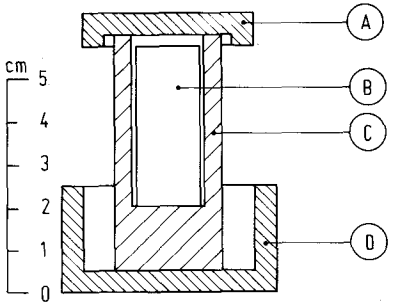

Fig. 4. Experimental set-up for the crucible test. A: Graphite lid; B: Compressed Al-cryolite cylinder; C: Test crucible; D: Graphite containment vessel.

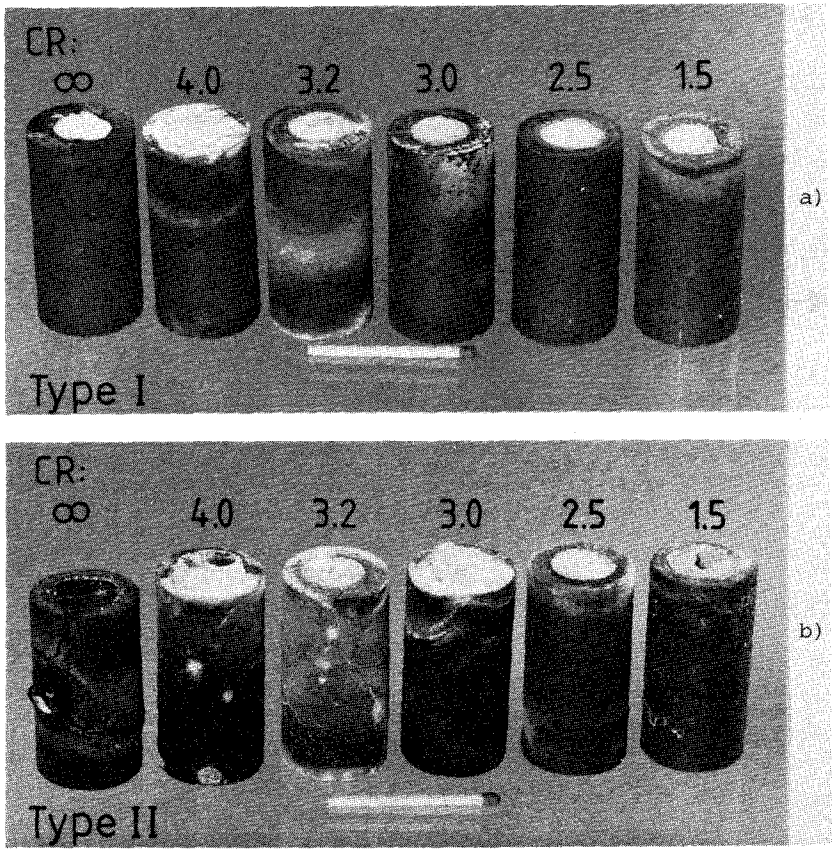

Fig. 5. Seam mix crucibles after test. Test conditions are 3.5h at 1000°C. Cryolite ratios (CR) are indicated.
a. Type I
b. Type II.

the conditions found at the metal-carbon interface in aluminium reduction cells. A thin layer of cryolite is always found (16) at the interface between the molten aluminium and the carbon lining.

The test took place in a vertical Kanthal wound furnace under a nitrogen atmosphere with a holding time at the upper temperature of 3.5h. Both types of seam mixes were tested with six different CR's at 1000°C. They were CR = ∞(NaF), 4.0, 3.2, 3.0(Na_3AlF_6), 2.5 and 1.5 (Fig. 5). Pure cryolite has a melting point of 1010°C so this composition and those closest to it were also tested at 1040°C which is well above the liquidus temperature. Tests were also performed at 950°C which is well below all liquidus temperatures except for the most acid composition (CR = 1.5).

The results are listed in Table 3. Figure 5a shows the series performed

Table 3. Effect of sodium penetration upon carbon crucibles fabricated from cold seam mixes.

CR	Mol% Na_3AlF_6	Weight% Na_3AlF_6	Type I	Type II
∞(NaF)	0	0	✱	✱✱✱
4.0	50.0	83.3	✱	✱✱
3.2	83.3	96.2	-	✱✱
3.0(Na_3AlF_6)	100	100	-	✱
2.5	83.3	92.6	-	✱
1.5	50.0	71.4	-	-

✱✱✱ : Extreme cracking and exfoliation
✱✱ : Heavy cracking
✱ : Moderate cracking, hair line cracks
- : No effect.

for Type I seam mix at 1000°C. Small hairline cracks are observed only with the two most basic compositions (CR = ∞, 4.0). The visual effect of sodium swelling and penetration is much more dramatic in Figure 5b which shows a similar series of experiments performed with the Type II cold seam mix. The cracking and exfoliation is extensive for the most basic compositions. Cracks are even found with acidic mixtures, only the specimen containing the most acidic melt (CR = 1.5) shows no sign of cracking. A change of temperature to 1040°C or 950°C gave no qualitative differences from those described above.

Sodium liberated according to reaction (1) will continuously diffuse into the carbon lattice. Thus, more sodium is generated than that to be expected from equilibrium considerations alone. Conditions may resemble those obtained when the carbon material is subjected to a low sodium vapour pressure. Additional complications due to the crystallization pressure of melt constituents (1) is not expected at these isothermal conditions, but a possible effect from the formation and growth of Al_4C_3 in the carbon materials (5,6) may be present. Characteristic yellowish deposits were sometimes observe

Similar conclusions may be drawn from these experiments as previously given for the action of sodium vapour alone. Despite its poorer crushing strength the Type I carbon is superior with respect to cracking and disintegration under conditions which may exist in aluminium reduction cells.

Electrochemical sodium generation

Direct deposition of aluminium at the cathode

$$Al^{3+} + 3e^- \rightarrow Al \qquad (3)$$

inheres also a co-deposition of sodium either by direct reduction

$$Na^+ + e^- \rightarrow Na(\text{in Al}) \qquad (4)$$

or by the equilibrium chemical reaction (1). Reaction (4) could alternatively be the first step followed by the reversal of reaction (1). It has not been possible to distinguish between these mechanisms (17) but the net effect, however, is that sodium is always present during the electrolysis.

The penetration of sodium and electrolyte was therefore studied in a reversed polarity apparatus shown in Figure 6. The test specimens were about 70 mm long and machined to a diamter of 25 mm. The machining was done after pressing and baking in order to remove the enrichment of fine particles near the surface. The carbon cylinder to be tested (B) served as the cathode. It was fastened to a graphite supporter (A) which could be rotated during electrolysis. Only 2 mm of the cylinder was submerged in the melt (D) but the rotation (200 rpm) gave satisfactory stirring of the electrolyte. A thermocouple (C) protected by a graphite tube recorded the temperature. The graphite crucible (E) served as the anode and electrical connection was achieved through a graphite supporter (F). The experiments were performed in a Kanthal wound vertical tube furnace under a nitrogen atmosphere. Constant current was achieved by means of a Hewlett-Packard Harrison 6439B DC power supply.

The rate of sodium penetration into the cathode is a function of current density, cryolite ratio (CR) and time of electrolysis. Due to the rapid sodium migration most experiments were performed at low current densities (~ 0.15 A cm^{-2}) or short time of electrolysis (≤ 4h). All experiments were performed at 1000°C. In addition to the given CR's all electrolytes contained 5 wt% Al_2O_3 and 5 wt% CaF_2.

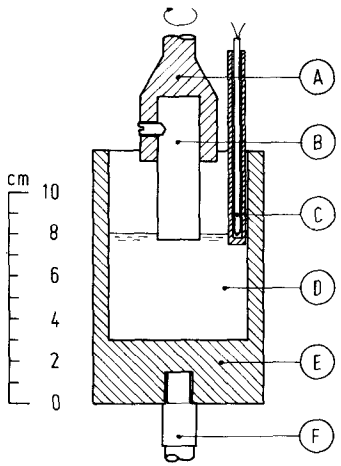

Fig. 6. Reversed polarity apparatus. A: Graphite supporter; B: Test specimen (cathode); C: Thermocouple; D: Cryolite melt; E: Graphite crucible (anode); F: Graphite supporter.

Swelling and cracking of the electrodes were not as pronounced as in the previous experiments, but cracks could sometimes be seen when electrodes of Type II mix were cut open after prolonged electrolysis in the most basic bath (CR = 4.0). The penetration of sodium was simply measured by cutting the electrode along its axis and pressing the exposed surface against a paper wetted with phenolphthalein acid-base indicator. Exposed sodium at the surface will react with moist air turning the indicator red.

Figure 7 shows the penetration determined by this technique for 4 samples of Type II after 0.5, 1, 2 and 4 hours of electrolysis. Although this quick and easy test does not give quantitative information about the concentration profile it gives a very clear visual picture of the penetration depth. In a subsequent paper we will also give concentration profiles determined by X-ray fluorescence but here only the penetration depth to a certain Na concentration as determined from the phenolphthalein test is considered.

The solution to Fick's law for diffusion along the X-axis in an infinite solid and where the supply of the diffusing species is constant (infinite reservoir) yields a linear relationship between the square of the penetration depth (for a constant concentration) *versus* time (18). Figure 8 gives the penetration depth for Type I, Type II and AUC graphite for CR= 4.0. For Type II the penetration for CR = 1.5 is also given. The square of the penetration depth is plotted *versus* time. The figure illustrates that increased graphitization and decreased cryolite ratio slows down the penetration. Experimental results might be somewhat scattered, both due to the inhomogeneity of the material and errors in determination of the position of the sodium front in the carbon rod. In spite of this, it is illustrative to use the slope on Figure 8 to calculate the time to penetrate 30 cm for the "worst" and "best" case. It is found that 30 cm penetration takes 13 days for Type II seam mix while it takes 300 days for AUC graphite, both examples calculated for CR = 4.0.

The porosity of the carbon material is greatly affected by the electrolysis. Figure 9 shows the integral pore size distribution before and after electrolysis for both carbon materials used as cathodes. The samples were taken from carbon rods which had been subjected to a cathodic current density of 0.15 A cm^{-2} for 4h at 1000°C (CR = 4.0). A slice of the electrode (<5mm, close to the surface in contact with the electrolyte) was analyzed in a Carlo Erba 1520 mercury porosimeter. The densities increase from 1.50 to 1.91 g cm^{-3} in Type I and from 1.41 to 1.80 in Type II carbon, while the porosity simultaneously drops from 18.6 to 7.8% and from 14.4 to 7.2% for Type I and Type II, respectively. From Figure 9 it can be seen that pores down to a radius of 0.3 μm is affected by the migrating bath.

This decrease in porosity is mainly due to migration of electrolyte into the porous binder material at the grain boundaries. Carbon specimens which had been subjected to the sodium vapour above a cryolite(CR=4.0) melt - aluminium melt (reaction (1)) did not display this large decrease in porosity although sodium was found throughout the material.

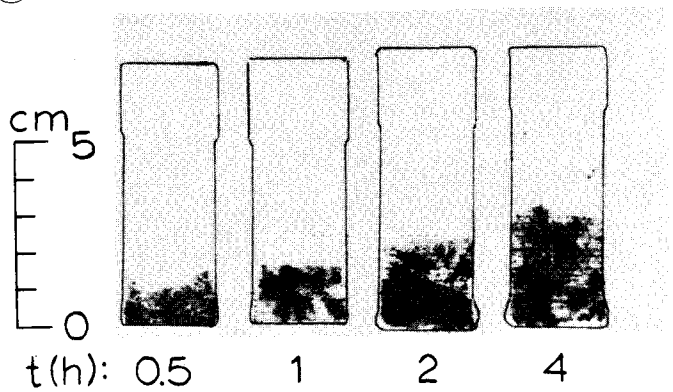

Fig. 7. Sodium penetration as displayed by the phenolphthalein test for a series of Type II cathodes.

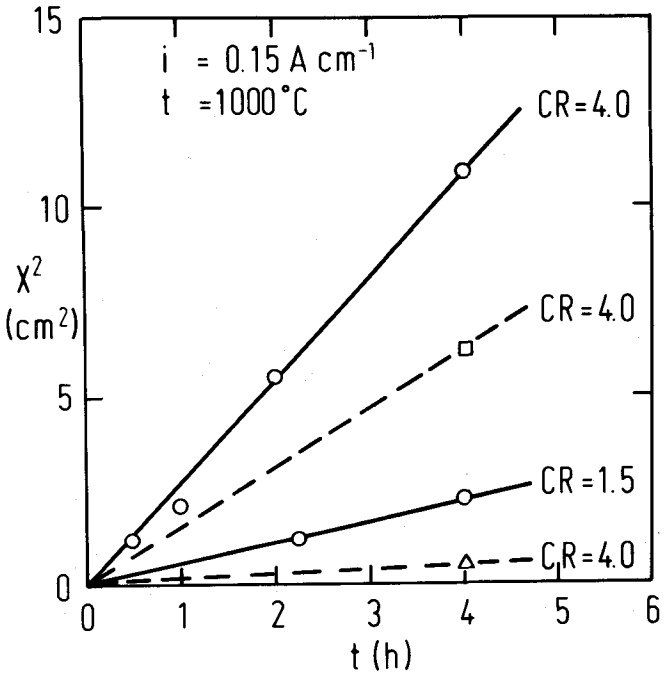

Fig. 8. Plots of the square of the sodium penetration front *versus* time of electrolysis. Cryolite ratio (CR) of bath is given.
□ : Type I
o : Type II
Δ : AUC graphite.

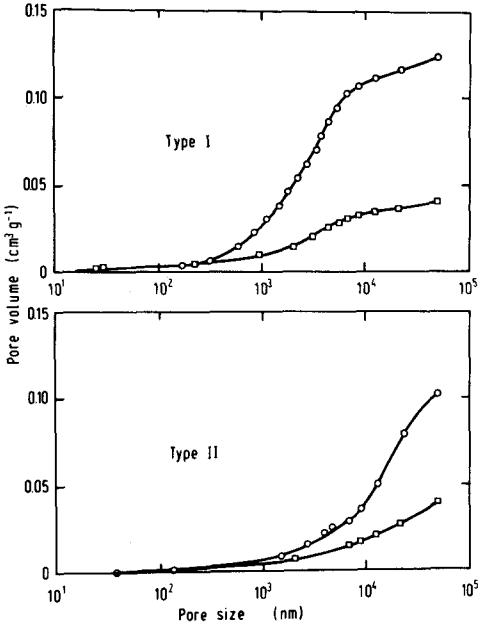

Fig. 9. Integral pore size distribution in Type I and Type II carbons.
o : Before electrolysis
□ : After electrolysis.

Mechanism of Sodium and Electrolyte Penetration

Electron microprobe analyses support the suggested mechanism of sodium migrating by diffusion through the carbon lattice (6) and not as a vapour predominantly transported through the pores (9). The analysis was performed on an Applied Research Laboratories scanning electron microscope quantometer (SEMQ). Figure 10 shows electron microprobe pictures (electron, Na, Al, F, X-ray emission) of a Type II specimen which has been used as a cathode in a cryolite melt (reversed polarity experiments as previously described). The electrode has been cut along its axis and polished. The photographs in Figure 10a have been taken from an area 3 cm above electrolyte level and the outline of a nearly rectangular anthracite grain is evident on the electron picture (upper left). It is seen that only sodium has penetrated this far (upper right). Moreover, the sodium X-ray emissions (which density is approximately proportional to the Na concentration) show that sodium has no preference for the more porous grain boundaries or their closest surroundings. The aluminium and fluorine X-ray emissions (lower row) are only due to some aluminium content in the coke ash and background noise.

Figure 10b is taken from a part closer to the electrolyte surface (about 0.5 cm above melt level). The electron image (upper left) shows some dense anthracite grains with a grain boundary originally filled with more porous material running diagonally across. The Na X-ray picture (upper right) also here show sodium within the anthracite grains but with a significant enrichment in concentration at the grain boundaries. Simultaneously, aluminium and fluorine (lower row) show emissions originating only from the porous binder material. It is evident that although sodium has penetrated the entire lattice, the cryolite melt is restricted to the porous matrix of the binder fraction and the grain boundaries.

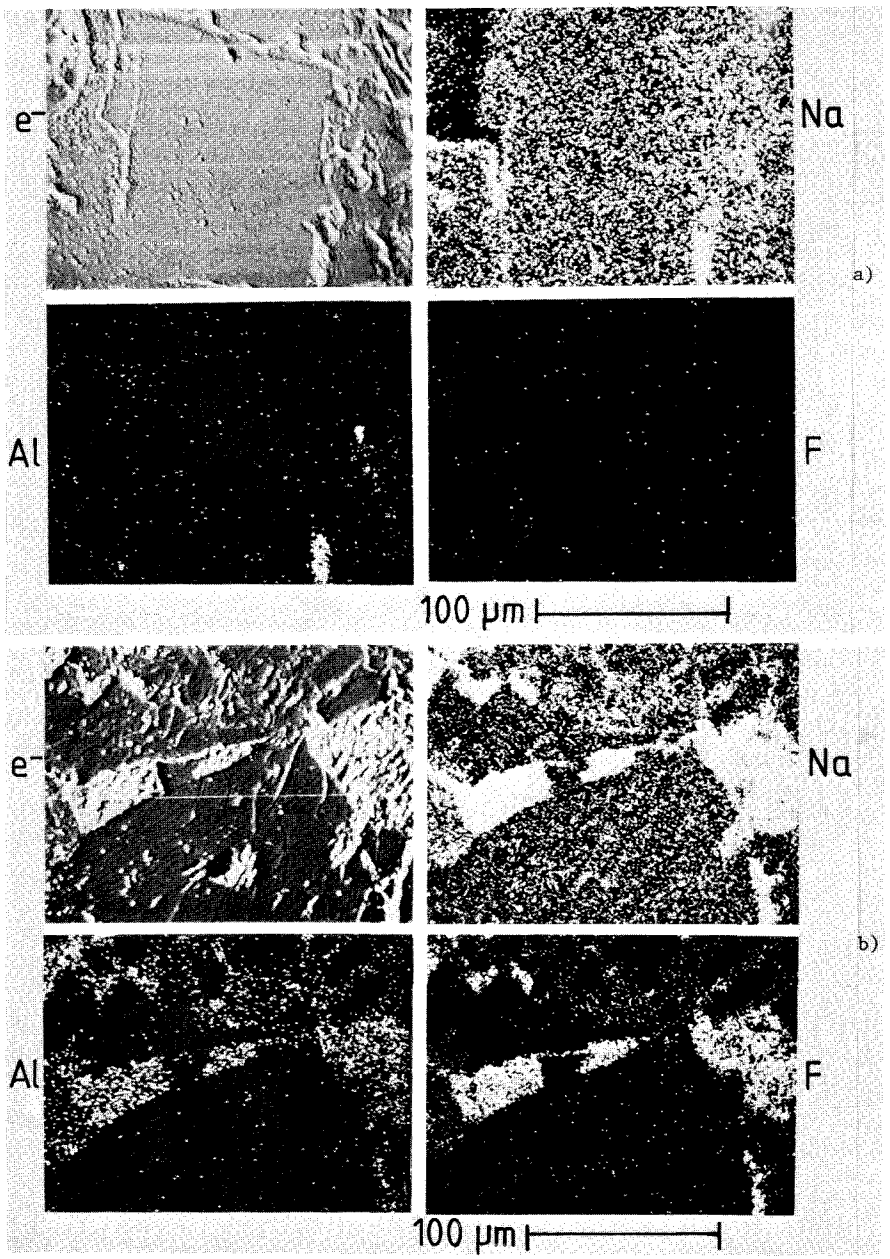

Fig. 10. Electron microprobe analysis from the interior of a Type II carbon cathode after electrolysis (reversed polarity apparatus). Clockwise from upper left: Electron image, Na, F and Al X-ray emissions.
a) 3 cm above electrolyte level
b) 0.5 cm above electrolyte level.

The conclusion is that when a cathodic potential is applied to the carbon, a sodium wave will first pass through the material followed by migrating electrolyte (9) which only has access to the porous parts of the material. The sodium intercalation process probably changes the wetting characteristics of the carbon material, thus enabling the bath to penetrate.

Acknowledgement

We wish to thank Mrs. Bente Bøe for experimental assistance. Financial support from *Norges Teknisk-Naturvitenskapelige Forskningsråd* and the Norwegian aluminium industry is gratefully acknowledged.

References

1. Sørlie, M. and Øye, H.A., Metall, submitted.
2. Belitskus, D., 3rd. Yugoslav Symposium on Aluminium, Ljubljana, 1978, p. 127.
3. Belitskus, D.L., Dell, M.B. and Farrah, G.H., Light Met., Proc. Sess. AIME Annu. Meet. 108th (1979) 647.
4. Rydland, U., Internal Report, Institutt for uorganisk kjemi, Universitetet i Trondheim, Norges tekniske høgskole, Norway, 1978.
5. Grjotheim, K., Næumann, R. and Øye, H.A., Light Met., Proc. Sess. AIME Annu. Meet., 106th (1977) 233.
6. Dewing, E.W., Trans. Met. Soc. AIME 227 (1963) 1328.
7. Rapoport, M.B. and Samoilenko, V.N., Tsvetn. Met. 30(2) (1957) 44.
8. Wilkening, S., Proc. London Int. Carbon Graphite Conf., 5th (1978) 725.
9. Dell, M.B., Extractive Metallurgy of Aluminium, Vol. 2, ed. by Gerard, G., Interscience Publishers, New York, 1963, p. 403.
10. Krol, L., Proc.-Ironmaking Conf. 37 (1978) 599.
11. Halpin, M.K. and Jenkins, G.M., Proc. Roy. Soc. Lond. A 313 (1969) 421.
12. Asher, R.C., J. Inorg. Nucl. Chem. 10 (1959) 238.
13. Pflugmacher, I. and Boehm, H.P., Conf. Ind. Carbons Graphite, Pap., 3rd (1970) 62.
14. Hooley, J.G., Garby, W.P. and Valentin, J., Carbon 3 (1965) 7.
15. Tingle, W.H., Petit, J. and Frank, W.B., Aluminium 57 (1981) 286.
16. Dorward, R.C., Met. Trans. 4 (1973) 386.
17. Grjotheim, K. and Welch, B.J., Aluminium Smelter Technology, Aluminium-Verlag GmbH, Düsseldorf, 1980, p. 67.
18. Tiselius, A., Z. phys. Chem. 169A (1934) 425.